ACS APPLIED MATERIALS & INTERFACES

www.acsami.org

Research Article

Bio-Inspired Bianisotropic Magneto-Sensitive Elastomers with Excellent Multimodal Transformation

Jingyi Zhang, Yu Wang,* Huaxia Deng, Chunyu Zhao, Yanan Zhang, Haiyi Liang, and Xinglong Gong*

Cite This: *ACS Appl. Mater. Interfaces* 2022, 14, 20101−20112

Read Online

ACCESS | Metrics & More | Article Recommendations | Supporting Information

ABSTRACT: Magneto-sensitive soft materials that can accomplish fast, remote, and reversible shape morphing are highly desirable for practical applications including biomedical devices, soft robotics, and flexible electronics. In conventional magneto-sensitive elastomers (MSEs), there is a tradeoff between employing hard magnetic particles with costly magnetic programming and utilizing soft magnetic particle chains causing tedious and small deformation. Here, inspired by the shape and movement of mimosa, a novel soft magnetic particle doped shape material bianisotropic magneto-sensitive elastomer (SM bianisotropic MSE) with multimodal transformation and superior deformability is developed. The high-aspect-ratio shape anisotropy and the material anisotropy in which the magnetic particles are arranged in a chainlike structure together impart magnetic anisotropy to the SM bianisotropic MSE. A magneto-elastic analysis model is proposed, and it is elucidated that magnetic anisotropy leads to peculiar field-direction-dependent multimodal transformation. More importantly, a quadrilateral assembly and a regular hexagon assembly based on this SM bianisotropic MSE are designed, and they exhibit 2.4 and 1.7 times the deformation capacity of shape anisotropic samples, respectively. By exploiting the multidegree of freedom and excellent deformability of the SM bianisotropic MSE, flexible logic switches and ultrasoft magnetic manipulators are further demonstrated, which prove its potential applications in future intelligent flexible electronics and autonomous soft robotics.

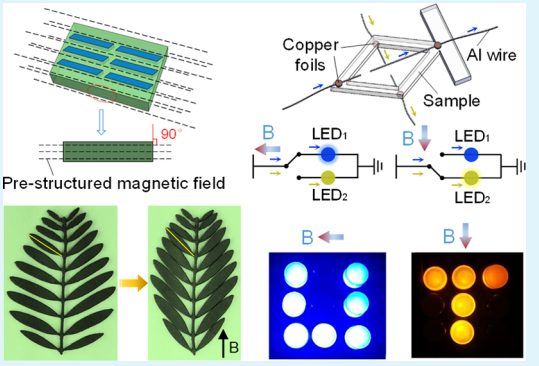

KEYWORDS: *magnetic properties, anisotropy, shape morphing, magnetic actuation, composites*

1. INTRODUCTION

For creating more advanced materials to meet people's requirements, research in chemistry,[1] mechanics,[2] and physics has drawn great interest in the development of bionic actuators,[3] sensors,[4] or autonomous robots,[5] especially the realization of new functions mimicking biological systems. By imitating the shape or internal structure of natural creatures,[6] the materials are endowed with excellent properties, making them intelligently respond to external stimuli such as force,[7,8] moisture,[9,10] temperature, etc. Among these studies, soft bionic smart materials have attracted more attention because of the advantages of low modulus, strong adaptability, high degrees of freedom, and noiseless locomotion compared with rigid materials.[11,12] For instance, the parthenocissus paw-shaped hydrogel has outstanding adhesion ability and acts as a drug microcarrier.[13] According to the asymmetric volume change of sunflower tissues, a superelastic body whose chamber is filled with liquid is designed to be an untethered soft actuator with a massive driving stroke.[14] An artificial muscle that consists of a flexible electrothermal film and a liquid-crystal elastomer is presented to program soft electrically actuated robotics.[15] Hence, imitating natural materials can provide an effective method to design more intelligent soft materials and pave the way for applications.

Magneto-sensitive elastomer (MSE) is a smart soft material composed of micron-sized magnetic particles and a polymer matrix. Depending on whether the magnetic particles are arranged in chains in the matrix, they are divided into material anisotropic MSE and material isotropic MSE (Figures S1−S3).[16,17] Under the excitation of an external magnetic field, the interactions of the particles, the matrix, and the magnetic field cause MSE reversible morphing and locomotion.[18] As compared with the smart polymeric composites that respond to other stimuli, such as light,[19,20] electric,[21,22] and pneumatic,[23−25] MSEs have the characteristics of good biocompatibility, permeability, wireless control, fast response, and nonlocal modulation, finding broad applications in soft robots,[26] flexible electronics,[27,28] and active metamaterials.[29−31] The efficiency and function of a device based on MSE materials are determined by their on-demand and multimodal deformability. Therefore, the exploration of MSE

Received: February 25, 2022
Accepted: April 11, 2022
Published: April 20, 2022

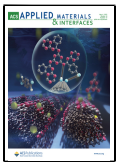

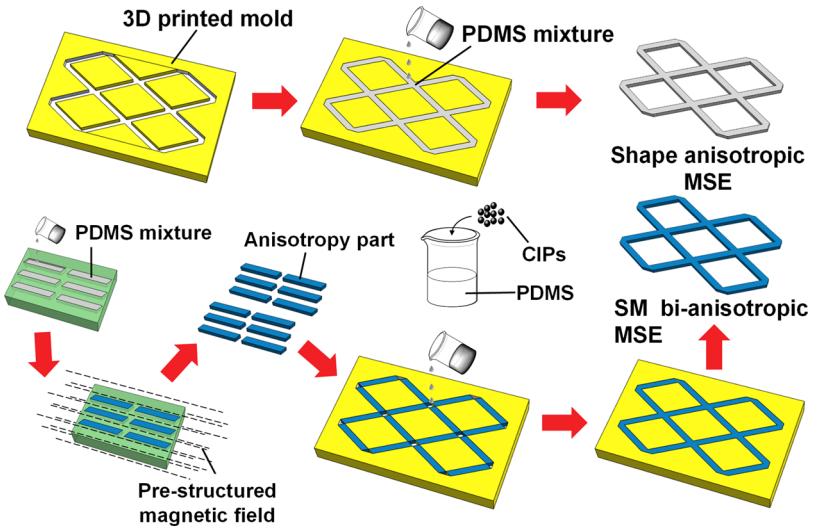

Figure 1. Preparation process of shape anisotropic MSE sample and shape material bianisotropic MSE sample.

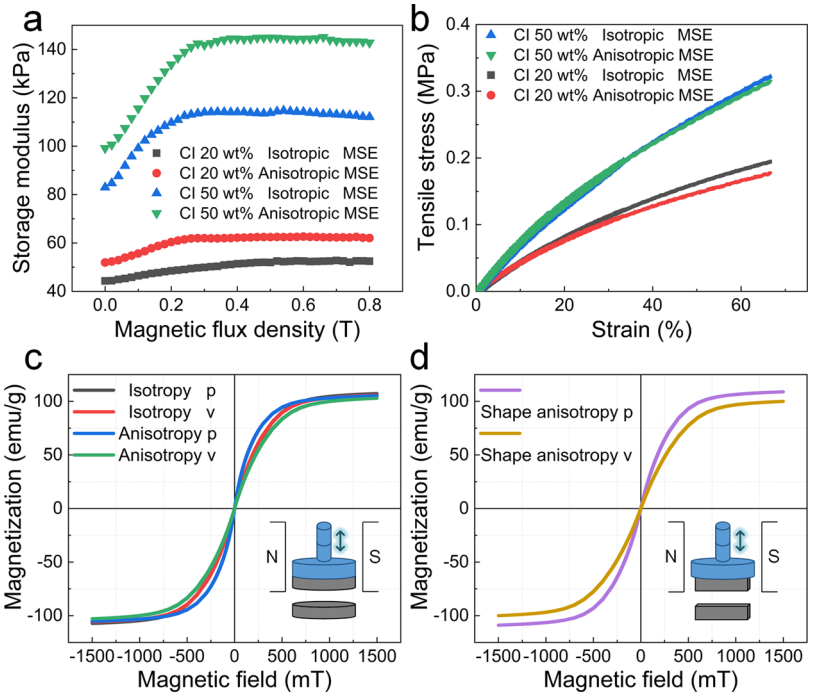

Figure 2. Physical properties of anisotropic MSE. (a) Magnetic field-dependent shear storage modulus of material isotropic and anisotropic MSEs with different carbonyl iron powder contents. (b) Quasi-static tensile stress−strain curve. (c) Magnetization results of disk material isotropic MSE and material anisotropic MSE. (d) Magnetization results of shape anisotropic MSE whose long axis is parallel or perpendicular to the direction of the tested magnetic field.

materials with multiple shape changes and large actuation strain is highly desired.[32,33]

In previous studies, MSEs embedded with ferromagnetic particles were prepared, which exhibited various complex transformations and motions attributed to the magnetization orientation of magnetic particle mismatching to the direction of the applied magnetic field.[34,35] The hard magnetic particle-based MSE can show obvious deformation using a small magnetic field.[36−38] However, employing a large premagnetization magnetic field to program the magnetization of the hard magnetic particles during the fabrication is requisite. Moreover, the hard magnetic particle-based MSE has a self-magnetic interaction, which will affect its initial and deformed configurations.[11] To tackle these issues, the material anisotropic MSEs with soft magnetic particles are explored.[39,40] The magnetically induced deformation is caused by the tendency of particle chains to align in the direction of the external magnetic field.[41] However, MSEs made of soft magnetic particle chains compromise the complex and large deformation.[42]

Herein, inspired by the shape and stress behavior of mimosa, we fabricate a soft magnetic particle-embedded shape material bianisotropic MSE (SM bianisotropic MSE) with a high aspect ratio using a small prestructured magnetic field. The proposed preparation method is low-cost, simple, and universal. This innovative SM bianisotropic MSE has enhanced magnetic

https://doi.org/10.1021/acsami.2c03533
ACS Appl. Mater. Interfaces 2022, 14, 20101−20112

anisotropy and thus exhibits excellent magneto-deformation performance with a fast response time, a multitransformation mode, multidegrees of freedom, and a larger deformation amplitude compared to shape anisotropic MSE. To explain the magnetic deformation behavior, a theoretical model based on energy variation is developed, and finite element analysis is conducted to complement and validate the experiments. Further, we demonstrate that the anisotropic multimodal large deformation offered by the promising SM bianisotropic MSE can be exploited for potential applications in flexible magnetically controlled electronics and next-generation intelligent soft robotics.

2. RESULTS AND DISCUSSION

2.1. Fabrication of SM Bianisotropic MSE. In this paper, the MSE with randomly distributed particles is defined as the material isotropic MSE. The material anisotropic MSE is the MSE whose particles are arranged in chains. Moreover, the "shape anisotropic MSE" represents the material isotropic MSE with shape anisotropy of a large length−width ratio. The "SM bianisotropic MSE" represents the material anisotropic MSE with shape anisotropy of a large length−width ratio.

The strategy for anisotropic MSE preparation is a 3D printing template sacrifice. The precursor, composed of poly(dimethylsiloxane) (PDMS) embedded with carbonyl iron (CI) particles, is poured into a predesigned mold. The shape anisotropic MSE is obtained once the precursor is vulcanized and demolded. During the preparation of the SM bianisotropic MSE, anisotropic parts are obtained by applying a prestructured magnetic field to the precursor. Subsequently, these components are assembled into an SM bianisotropic MSE using a precursor (Figure 1). PDMS that has a low rubbery modulus and CI microparticles that possess high magnetic saturation and low hysteresis are combined to yield good elasticity and strong magnetic properties of MSE.

Material isotropic and material anisotropic MSEs are prepared to characterize their mechanical and magnetic properties. Figure 2a shows the magnetorheological properties of the material isotropic and material anisotropic MSEs with 20 and 50 wt % CI. The initial shear storage moduli are 44 and 83 kPa for isotropic samples with 20 and 50 wt % CI. When the external magnetic flux density increases from 0 to 800 mT, the storage moduli reach 52 and 112 kPa, respectively. For anisotropic samples, their initial storage modulus is slightly higher than that of isotropic samples with the same particle loading. However, the magnetic saturation modulus (the storage modulus under a 0.8 T magnetic field) of anisotropic samples is much larger than that of isotropic samples. When the CI mass fraction is 50%, this phenomenon is obvious. A small difference in the initial moduli between material isotropic and material anisotropic samples indicates that the anisotropic one retains excellent flexibility. The remarkable distinction in the magnetic saturation modulus proves that the anisotropy of MSE enhances the response to the magnetic field. Figure 2b shows a tensile stress−strain curve of the isotropic and anisotropic MSEs with 20 and 50 wt % CI. During the loading process of various strains, all of the samples display good elastic deformability to allow large actuation. The Young's modulus of the sample increases with increasing CI content, which allows MSE tunable actuating performance. The CI contents of the samples in the subsequent experiments are 50% unless specified.

Figure S4a shows the hysteresis loops of pure CI and a sample with 50 wt % CI. Both pure CI and the sample hardly have magnetic hysteresis. The sample has low coercivity and low remanence. The magnetizations of the material isotropic sample and the material anisotropic 90° sample under different magnetic field directions are shown in Figure 2c. For the material anisotropic sample, the result when the internal particle chain orientation is parallel to the test magnetic field direction is named "anisotropy p" and the result after the sample is rotated 90° is named "anisotropy v". The "isotropy p" and "isotropy v" represent the magnetization results of the the material isotropic sample. Figures 2c and S4b display that the "isotropy p" curve and the "isotropy v" curve of the material isotropic sample are completely coincident. For the anisotropic sample, the "anisotropy p" curve and the "anisotropy v" curve coincide at the saturation magnetic field. However, under a weak magnetic field, the "anisotropy p" curve is the highest and the "anisotropy v" curve is the lowest (Figures 2c and S4c), which proves that the material anisotropy endows MSE with magnetic anisotropy, the characteristics of sensitivity to the direction of the external magnetic field. The different magnetizations of the shape anisotropic MSE sample are shown in Figure 2d. The results that the long axis of the sample is parallel to and perpendicular to the external magnetic field are named "shape anisotropy p" and "shape anisotropy v", respectively. Interestingly, the longitudinal direction of the sample parallel to the external magnetic field direction (shape anisotropy p) will lead to a higher magnetization. Therefore, shape anisotropy of MSE may also lead to magnetic anisotropy.

Figures 3 and S5 present several shape anisotropic MSEs, including some common architectures such as a rhombic-

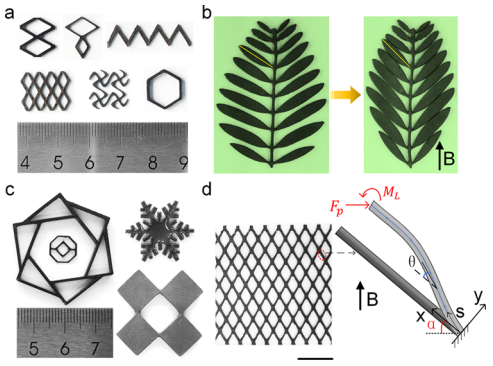

Figure 3. (a) Various millimeter-scale netted-shape anisotropic MSEs prepared by the template sacrifice method. (b) Shape anisotropic MSEs resembling mimosa. (c) Samples with interesting shapes. (d) Magneto-deformation mechanism of hepatic lobule distribution-inspired anisotropic MSE. Scale bar is 10 mm.

shaped grid, a regular honeycomb, an arc pattern, a re-entrant honeycomb, and a chiral lattice and various bionics shapes such as snowflakes, kirigami, and mimosa. These diverse shape anisotropic MSEs from linear to curved construction structures or from truss to paper structures are successfully constructed, well exhibiting the versatility of the 3D printing template sacrifice method.

Mimosa is a subshrubby herb. A compound leaf is composed of many microphyllous leaves arranged in feathers on both sides of the leaf axis. These microphyllous leaves are slender and will deform immediately when touched by an external

https://doi.org/10.1021/acsami.2c03533
ACS Appl. Mater. Interfaces 2022, 14, 20101−20112

force. As shown in Figure 3b, the strip-shaped anisotropy MSEs like the microphyllous leaves are assembled into a compound leaf of mimosa. After applying a magnetic field, will the MSEs deform like the microphyllous leaves? The experimental result shows that the answer is yes. The shape anisotropy equips MSE with magnetic anisotropy, the capability to perceive the direction of the magnetic field (Figure 2d). When the longitudinal direction of the shape anisotropic MSE is consistent with the direction of the external magnetic field, the magnetization is the highest and the magnetic potential energy is the lowest.[43] The longitudinal direction of shape anisotropic MSEs is the direction of the microphyllous leaves' leaf axis. The direction of applied magnetic field is along the leaf axis of the compound leaf. Therefore, the shape anisotropic MSEs would bend into the magnetic field direction as if the microphyllous leaves are activated by an external force.

The deformation of shape anisotropic MSE could be simplified as cantilever bending. Inspired by the hepatic lobule structure (Figure 3d), a network MSE for transferring the cantilever bending to the whole architecture stretching or contracting is assembled.

2.2. Transformation Mechanism of SM Bianisotropic MSE. To analyze the deformation of the network MSE under a uniform magnetic field **B**, we select a representative volume element (RVE) for mechanical modeling according to the structural symmetry of the sample. The rectangular coordinate (x, y) and the curvilinear coordinate system (s, θ) are shown in Figure 3d. The free energy of RVE can be expressed as[44,45]

$$\Pi = \int_0^L \left\{ \frac{EI}{2}\left(\frac{d\theta}{ds}\right)^2 - bh\int_0^{\mathbf{B}} \mathbf{M}\cdot d\mathbf{B} \right\} ds - F_p \cdot u_L \tag{1}$$

Here, L and EI represent the length and bending stiffness of the RVE beam, $I = \frac{bh^3}{12}$, respectively, with b and h being the thickness and width, respectively. **B** and **M** are the magnetic flux density and the magnetization intensity, respectively. They are decomposed in a rectangular coordinate (the detail is included in Section S1)

$$\mathbf{B} = \mu_0 \mathbf{H}_0 = \begin{bmatrix} \mu_0 \mathbf{H}_0 \cos\beta \\ \mu_0 \mathbf{H}_0 \sin\beta \end{bmatrix} \tag{2}$$

$$\mathbf{M} = \begin{bmatrix} \chi_1 \mathbf{H}_0 \cos\beta \\ \chi_2 \mathbf{H}_0 \sin\beta \end{bmatrix} \tag{3}$$

where μ_0 and $\mathbf{H_0}$ are the vacuum permeability and the initial magnetic field intensity, respectively. χ_1 and χ_2 are the magnetic susceptibilities. β is the long axis of the beam to the direction of the magnetic field. $\beta = \pi/2 - \theta - \alpha$.

$\boldsymbol{F_p}$ and $\boldsymbol{u_L}$ are the horizontal reaction force and displacement at $s = L$.

$$F_p = (F_p\cos\alpha, F_p\sin\alpha) \tag{4}$$

$$u_L = \left(L - \int_0^L \cos\theta ds, \int_0^L \sin\theta ds\right) \tag{5}$$

Then, the free energy is derived as

$$\Pi = \int_0^L \left\{ \frac{EI}{2}\left(\frac{d\theta}{ds}\right)^2 - \frac{bh\mu_0 H_0^2}{2}[\chi_2\cos^2(\theta+\alpha) + \chi_1\sin^2(\theta+\alpha)] + F_p\cos\alpha\cos\theta - F_p\sin\alpha\sin\theta \right\} ds - F_p L\cos\alpha \tag{6}$$

The variation of the free energy is

$$\delta\Pi = -\int_0^L \left\{ EI\frac{d^2\theta}{ds^2} + \frac{bh\mu_0 H_0^2}{2}(\chi_1 - \chi_2)\sin(2\theta+2\alpha) + F_p\cos\alpha\sin\theta + F_p\sin\alpha\cos\theta \right\}\delta\theta ds + EI\frac{d\theta}{ds}\delta\theta\Big|_0^L \tag{7}$$

Considering the boundary conditions that $\theta(s = L) = 0$ and $\theta(s = 0) = 0$, the deformation equilibrium equation of RVE can be obtained.

$$EI\frac{d^2\theta}{ds^2} = -\frac{bh\mu_0 H_0^2}{2}(\chi_1 - \chi_2)\sin(2\theta+2\alpha) - F_p\cos\alpha\sin\theta - F_p\sin\alpha\cos\theta \tag{8}$$

Solving the equation

$$\frac{d\theta}{ds} = \pm\sqrt{\frac{bh\mu_0 H_0^2\Delta\chi}{2EI}\cos(2\theta+2\alpha) + \frac{2F_p}{EI}(\cos\alpha\cos\theta - \sin\alpha\sin\theta) + \frac{2\bar{C}}{EI}} \tag{9}$$

We denote $Q = \frac{bh\mu_0 H_0^2\Delta\chi}{2EI}$, $F_1 = \frac{2F_p}{EI}$, and $C = \frac{2\bar{C}}{EI}$. Then, we have

$$\frac{d\theta}{ds} = \pm\sqrt{Q\cos(2\theta+2\alpha) + F_1\cos(\theta+\alpha) + C} \tag{10}$$

Integrating the equation by s, we have

$$s(\theta) = \int_0^\theta \frac{d\theta}{\sqrt{Q\cos(2\theta+2\alpha) + F_1\cos(\theta+\alpha) + C}} \tag{11}$$

When $s = L$ and $\theta = \theta^* = 0$, we have

$$L = \int_0^{\theta^*} \frac{d\theta}{\sqrt{Q\cos(2\theta+2\alpha) + F_1\cos(\theta+\alpha) + C}} \tag{12}$$

Assuming that the length of RVE remains the same before and after the deformation, we have

$$f(\delta, \zeta, \alpha, L) = 0 \tag{13}$$

where δ and ζ are the x-direction and y-direction displacement at $s = L$, respectively. From eqs 5 and 11, they can be expressed as

$$\delta = L - \int_0^L \cos\theta ds = L - \int_0^{\theta^*} \frac{\cos\theta d\theta}{\sqrt{Q\cos(2\theta+2\alpha) + F_1\cos(\theta+\alpha) + C}} \tag{14}$$

https://doi.org/10.1021/acsami.2c03533
ACS Appl. Mater. Interfaces 2022, 14, 20101−20112

$$\zeta = \int_0^L \sin\theta \mathrm{d}s = \int_0^{\theta*} \frac{\sin\theta \mathrm{d}\theta}{\sqrt{Q\cos(2\theta + 2\alpha) + F_1\cos(\theta + \alpha) + C}} \quad (15)$$

Combining eqs 12−15, we can solve the unknown parameters F_1, C, δ, and ζ if the magnetic field Q is given. For particle-embedded MSE composites, the magnetic susceptibility cannot be accurately measured experimentally because of the unknown compact volume. However, according to the theoretical analysis, we have obtained that the deformation of the anisotropic MSE based on soft magnetic particles is not only related to the magnitude of the external magnetic field but also significantly affected by the sample's shape and boundary conditions.

2.3. Magnetic Actuation Deformation of Shape Anisotropic MSE. To demonstrate the deformability of shape anisotropic MSE, quadrilateral and hexagonal structures are designed and manufactured, as shown in Figures 4, 5, and S6. The thickness is 0.5 mm. The sample is fixed at the origin of the coordinates, and other positions are free. A uniform magnetic field is applied in the vertical and horizontal directions separately. The in-plane multimode deformations of shape anisotropic MSE under the external magnetic field are implemented by experiment and verified by the finite element method.

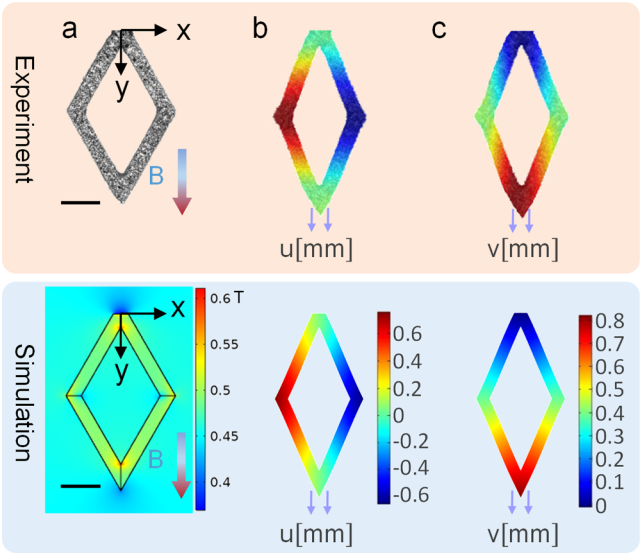

Figure 4. Magneto-deformation of rhombic-shaped anisotropic MSE under a vertical magnetic field. (a) Calculated magnetic flux density distribution on and around the sample. *x*-direction (b) and *y*-direction (c) displacement cloud images. Scale bar is 3 mm.

For quadrilateral-shaped anisotropic MSE, a slender configuration is obtained under the vertical direction magnetic field with amplitude $|B|$ = 450 mT (Figure 4a), having a symmetrical deformation about the y axis. The maximum displacement in the x-direction is about ±0.65 mm (Figure 4b). The maximum elongation in the y-direction is up to 0.82 mm (Figure 4c). Through strain results (Figure S7a),[46,47] it can be found that the sample is mainly compressed in the *x*-direction and tensioned in the *y*-direction. The shear strain cloud diagram reveals that the deformation of the quadrilateral sample is attributed to the beam bending. The finite element

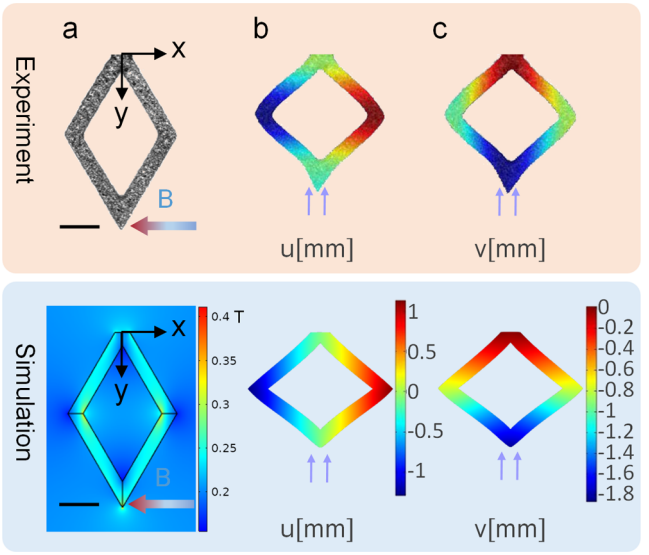

Figure 5. Magneto-deformation of rhombic-shaped anisotropic MSE under a horizontal magnetic field. (a) Calculated magnetic flux density distributions on and around the sample. *x*-direction (b) and *y*-direction (c) displacement cloud images. Scale bar is 3 mm.

calculation results shown in Figures 4b,c and S7b are in good agreement with the experimental results. Under a 450 mT horizontal magnetic field (Figure 5a), the quadrilateral-shaped anisotropic MSE deforms into a square experiencing about ±1.13 mm displacement in the x-direction (Figure 5b) and −1.87 mm maximum displacement in the y-direction (Figure 5c). The deformed strain results shown in Figure S7c depict that the positions with the largest tensile strain in the *x*-direction and the positions with the largest compressive strain in the *y*-direction are both at the beam junction. The shear strain demonstrates that the deformed square configuration is also the result of beam bending. The calculation results are shown in Figures 5b,c and S7d, respectively. The above results indicate that the shape anisotropic MSE can exhibit different deformations under a horizontal or vertical magnetic field. The transformation is essentially a combination of the bending of beams.

Under different magnetic flux densities, the deformations of the rhombic sample are recorded. The deflection increases with the magnetic flux density increasing (Video S1). The dynamic response of the sample to the vertical magnetic field with different magnitudes is tested. Figure S8a−c shows the variation of the excitation current and the *y*-direction displacement of the sample with time. Summarizing the displacement under different magnetic flux densities (Figure S8d,e), it is found that the response time of the deformation is about 300 ms (Figure S8f), indicating that the anisotropic MSE has a fast response time.

Next, we explore a shape anisotropic MSE with a honeycomb structure. Under the vertical magnetic field (Figure S6a), the sample is contracted by about ±1.11 mm in the x-direction (Figure S6b) and elongated by 2.18 mm in the y-direction (Figure S6c). The strain cloud diagrams (Figure S9a) show that the sample is subjected to compressive strain in the x-direction and tensile strain in the y-direction at the beam junction. The shear strain on the inclined beams of the sample is larger than that on the vertically oriented beams. According to the simulation results (Figure S9b), the vertical beams are slightly stretched in the y-direction, which indicates

https://doi.org/10.1021/acsami.2c03533
ACS Appl. Mater. Interfaces 2022, 14, 20101−20112

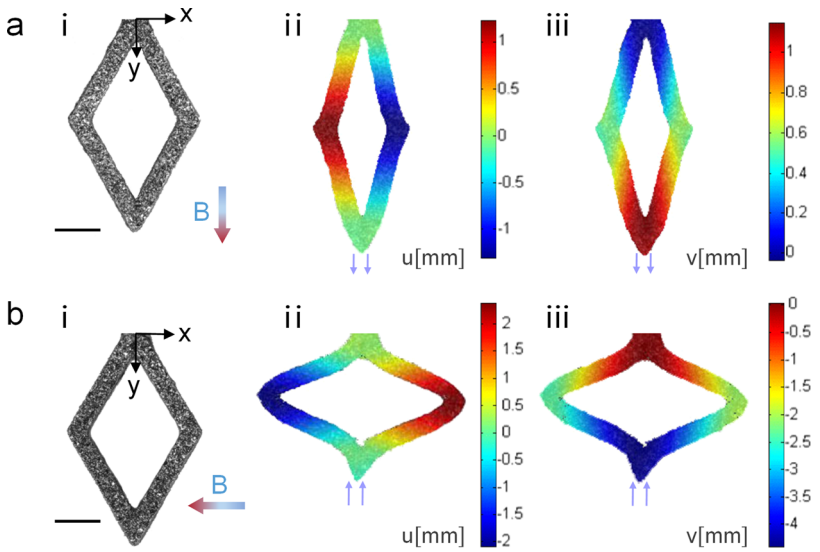

Figure 6. Magneto-deformation of rhombic SM bianisotropic MSE. (a) *x*-direction (ii) and *y*-direction (iii) displacement cloud images under a vertical magnetic field. (b) Displacement cloud images under a horizontal magnetic field. Scale bar is 3 mm.

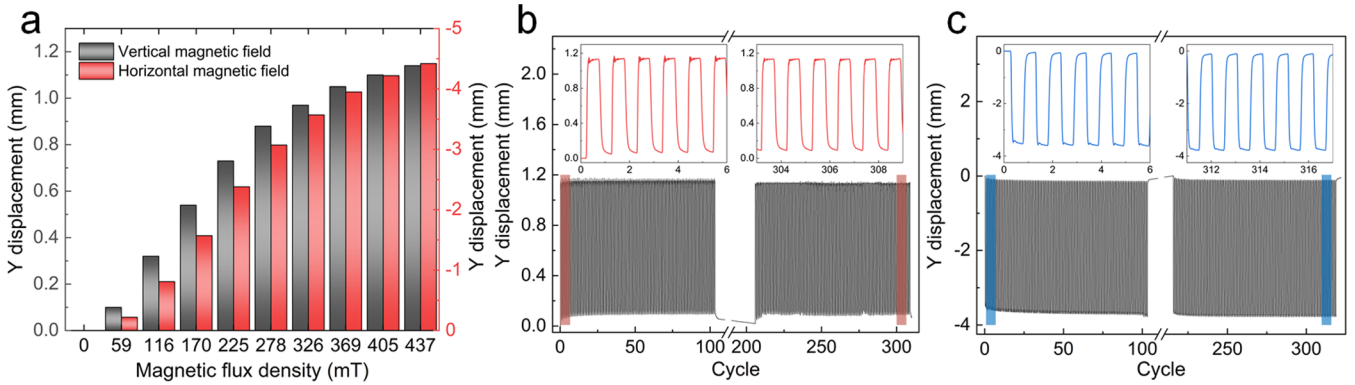

Figure 7. Deformation of the rhombic SM bianisotropic MSE. (a) *y*-displacements varying with the strengths of the applied magnetic field. *y*-direction displacement under a vertical (b) or horizontal (c) periodic square-wave magnetic field.

that they primarily play the role of connecting deformation. When the magnetic field is applied horizontally (Figure S6d), the sample exhibits another deformed configuration, with an extension of ±0.46 mm in the x-direction (Figure S6e) and a shrinkage of 1.03 mm in the y-direction (Figure S6f). The calculated results verify the experimental results well. It should be mentioned that during the deformation, the vertical beams are subjected to compression deformation in the *y*-direction and has stability problem (Figure S9d). Therefore, to ensure that the honeycomb structure is stable with a symmetrical deformed configuration, the magnetic flux density of the horizontal magnetic field is reduced to 232 mT. Moreover, the anisotropic deformation of a re-entrant honeycomb-shaped anisotropic MSE to the direction of the magnetic field is also studied, as shown in Figure S10. Under the magnetic field of 450 mT in different directions, the sample shows expansion and contraction behaviors, respectively.

2.4. Magnetic Actuation Deformation of SM Bianisotropic MSE. The previous anisotropic MSEs with different shapes have magnetic field-dependent multimode deformation. The deformation comes from the beam bending deformation imparted by the shape-induced magnetic anisotropy. As discussed previously, magnetic anisotropy also appears in the material anisotropic sample, which consists of particles arranged in chains in the matrix. Here, for increasing the magnetic anisotropy and deformability of MSEs, the shape material bianisotropic MSE is proposed through introducing the material anisotropic property into the shape anisotropic sample. As shown in Figures 6, S11, and S12, the SM bianisotropic MSEs with a thickness of 0.5 mm are applied with horizontal and vertical magnetic fields. The magnetic flux density is 450 mT. The quadrilateral sample stretches along the *y*-direction under the vertical magnetic field (Figure 6a) but shows a contracted pattern under the horizontal magnetic field (Figure 6b), exhibiting direction-dependent transformation of the magnetic field. Comparing Figure 4c and Figure 6a(iii), it can be found that the elongation of the SM bianisotropic sample is 1.4 times that of the shape anisotropic sample. In another configuration (Figures 5c and 6b(iii)), the tightening capability is improved by 1.4 times. The honeycomb SM bianisotropic sample is elongated by 3.69 mm in the y-direction under the vertical magnetic field (Figure S11c), which exhibits more significant deformation compared with the shape anisotropic sample shown in Figure S6c. Therefore, the SM bianisotropic MSEs have much superior magnetic field direction-dependent deformation.

The deformation amplitudes of the quadrilateral SM bianisotropic MSE under different magnetic flux densities are

https://doi.org/10.1021/acsami.2c03533
ACS Appl. Mater. Interfaces 2022, 14, 20101−20112

experimented (Figure 7a). The gray columns represent the maximum elongation displacements of the sample under different vertical magnetic fields. The displacement increases with the magnetic flux density increasing, but the growth rate gradually slows down. The maximum shrinkage displacements of the sample under horizontal magnetic fields are represented by red columns. The displacement shows a nonlinear positive correlation with magnetic flux density. Therefore, the deformation amplitude of SM bianisotropic MSE is not proportional to the strength of the magnetic field. The durability of the quadrilateral SM bianisotropic MSE is evaluated under a periodic square-wave magnetic field with a strength of 450 mT and a frequency of 0.5 Hz. Figure 7b,c shows that the *y*-direction displacement and the response speed of the sample are almost unaffected, experiencing 300 strong magnetic field cycles. It indicates that the SM bianisotropic MSE sample has durable magneto-deformation and would not be damaged by a long-time strong magnetic field.

MSE has been explored for logic gates due to potential applications in intelligent flexible electronics, alleviating the failure encountered in conventional rigid conductors.[48] Here, we demonstrate that the SM bianisotropic MSE with excellent multimode transformation can be used as a soft electronic switch. A quadrilateral sample is decorated with copper foils on its beam junction (Figure 8a(i)). Two Al wires fixed on the copper foils are used as a terminal pair of an LED circuit (Figure 8a(iii)). We apply a 286 mT horizontal magnetic field to deform the sample. As shown in Figure 8a(ii,iv), the terminal pair contacts and the blue LED lights up. Note that increasing the length of Al wires contributes to decreasing the sample displacement for connecting the circuit; then, the strength of the applied magnetic field can be decreased. We also demonstrate a normally closed switch using a hexagonal sample (Figure 8c). Under a 116 mT vertical magnetic field, a terminal pair is disconnected and the red LED is off. Due to the capability of response to the magnetic field direction, the quadrilateral sample is then mounted with another terminal pair connecting a yellow LED, which becomes a double-open switch (Figure 8b,d). The yellow LED lights up when a 286 mT vertical magnetic field is applied. Video S2 records the controls of these SM bianisotropic MSE-based electronic switches to the LEDs. Subsequently, nine quadrilateral samples are exploited to design a 3 × 3 LED switch array, which can display the alphabets "U" and "T". When applying the magnetic field, the terminal pair on a switch is connected and the LED lights up, which is represented by the "1" state. Without a magnetic field, the terminal pair is disconnected and the LED is off (represented by a "0" state). Figure S13 shows that integrating mode "U" and mode "T" into the switch array has three distinct coding states (U,T) = (1, 1), (1, 0), or (0, 1), corresponding to three types of switches. Through assembling these switches, the 3×3 LED array can show a "U" or "T" pattern in a horizontal or vertical magnetic field (Figure S13b). The programmable flexible switch based on the SM anisotropic MSE has wireless control, fast response speed, and robust function, showing potential in optoelectronic and optogenetic research.

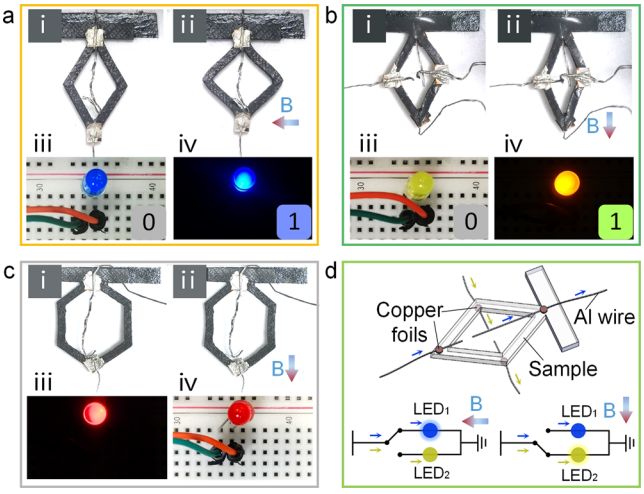

Figure 8. SM bianisotropic MSE as a logical magneto-control electronic switch. (a) In the absence (i) and presence (ii) of a horizontal magnetic field, the rhombic sample corresponds to circuit open (iii) and closed (iv). (b) The rhombic sample acts as another circuit switch in response to a vertical magnetic field. (c) The regular hexagon sample is designed as a normally closed circuit switch. (d) Schematic and circuit diagrams of the rhombic sample interspersed with wires.

2.5. Applications of SM Bianisotropic MSE for Object Manipulation. The untethered and reversible magneto-induced deformation response of MSE provides the capability to develop a magnetically controlled soft robot. For magnetic soft robots, higher degrees of freedom and larger displacements are desired. Utilizing the excellent deformability of the SM bianisotropic MSE, wrapping a magnet, and manipulating a heavy object can also be achieved. For comparison, a solid MSE and a reticulated SM bianisotropic MSE with the same size are prepared (Figure S14a). The two samples are held slowly near a small magnet with a plastic tweezer. The magnet instantaneously attaches to the solid sample, exhibiting an upward displacement (Figure S14b). Meanwhile, the SM bianisotropic sample completely envelops the magnet. Compared with the solid sample, SM bianisotropic sample actuates the magnet a more pronounced distance because it has small bending stiffness and great elasticity (Video S3).

A magnetically assisted flexible gripper based on the SM bianisotropic MSE is demonstrated. As shown in Figure 9, the PLA weight is 3 times the weight of the gripper and placed on the surface of an electromagnet. The gripper can lift and lay down the weight when there is no magnetic field, interlocking with the weight by its network structure. Unfortunately, the whole process stumbles, owing to the small bending stiffness of the sample. However, once assisted by the magnetic field of the electromagnet during the lifting process, the gripper is stretched closer to the weight (Figure 9a(i,ii)) and the lifting becomes easy thanks to the gripper's increased in-plane tension (Figure 9a(iii,iv)). Moreover, the gripper can fulfill the placing process under the magnetically controlled mode (Figure 9b and Video S4). Therefore, the SM bianisotropic MSE with great deformability and controllability shows potential in developing magnetic soft robots for minimally invasive surgery in the future.[49]

2.6. Electronic Applications of SM Bianisotropic MSE with 3D Multimode Deformation. As soon as a compound leaf of mimosa is touched (Figure 10a(i)), its microphyllous leaves not only bend in-plane along the leaf axis direction (Figure 10a(ii)) but also fold up with out-of-plane deformation, as shown in Figure 10a(iii). Here, the out-of-plane transformation of an SM bianisotropic MSE is further

https://doi.org/10.1021/acsami.2c03533
ACS Appl. Mater. Interfaces 2022, 14, 20101−20112

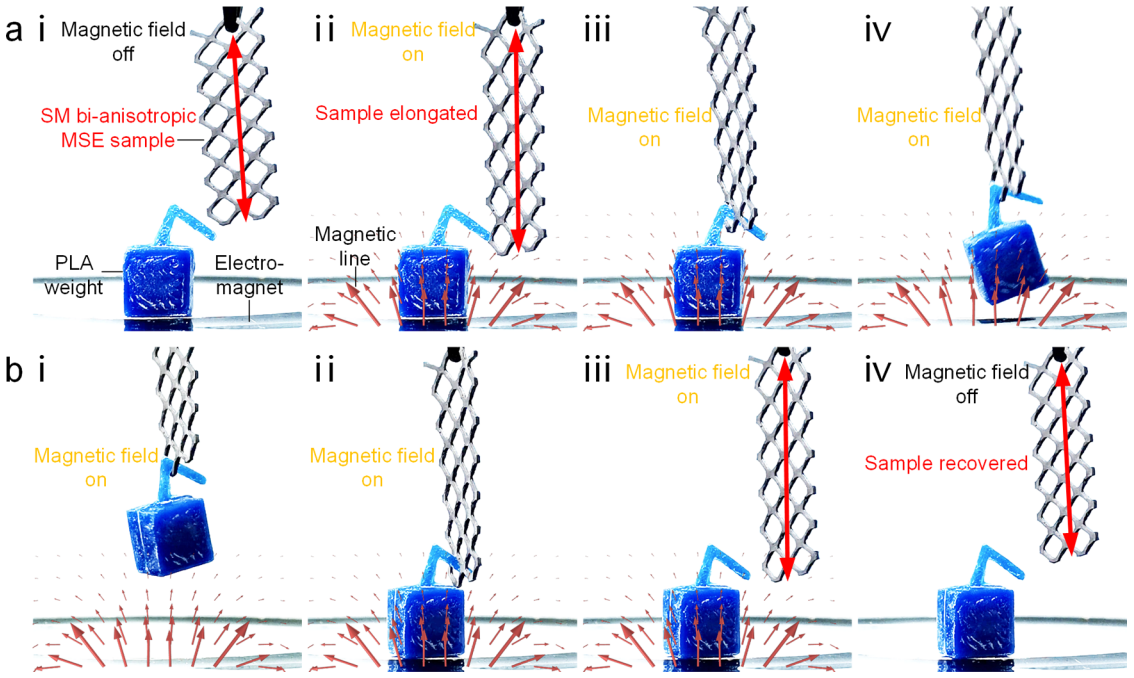

Figure 9. Process of SM bianisotropic MSE-based magnetically controlled gripper lifting (a) and placing (b) a PLA weight.

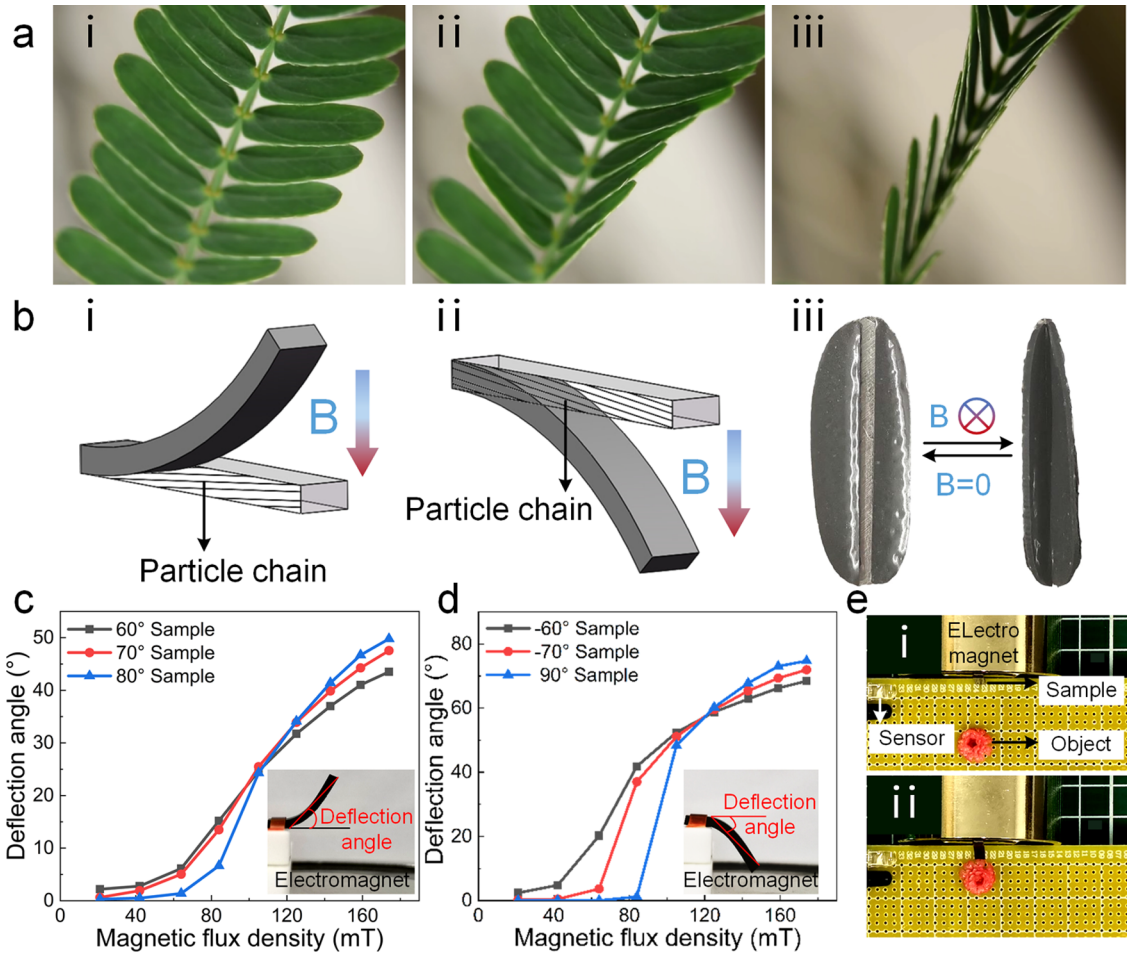

Figure 10. Out-of-plane deformation and application of SM bianisotropic MSE. (a) Process of the stimulated mimosa closing its leaves. (b) 3D deformation mechanism of SM bianisotropic MSE, which contains inclined particle chains. (c, d) Experimentally measured deformation angles of the samples with different particle chain orientations. (e) The sample with magnetically actuated off-plane deformation is connected with an infrared sensor to realize the defense function.

https://doi.org/10.1021/acsami.2c03533
ACS Appl. Mater. Interfaces 2022, 14, 20101−20112

researched by alternating the particle chain orientation at a certain angle with the longitudinal direction. The microstructure and fabrication of the SM bianisotropic MSEs with different particle chain orientations are detailed in Figures S1, S2, and S15. Figure 10b(i,ii) shows that the particle chains tend to the direction of the external magnetic field and the SM bianisotropic MSE sample exhibits upward or downward off-plane deformation dependent on the orientation of the particle chains. Figure 10b(iii) exhibits a structure that consists of two samples with different particle chain orientations. When applying an off-plane magnetic field, the structure folds like the mimosa due to the different deformations on both sides. After the magnetic field is removed, the structure resumes plane configuration, just like the mimosa returns to the initial state after a period of quietness.

The inset of Figure 10c shows the 80° sample bends upward suffering from a 174 mT magnetic field, and the deformation angle is defined. Figure 10c depicts that the deformation angle of the 60° sample is the largest when the magnetic flux density is less than 105 mT. However, when the magnetic flux density is greater than 105 mT, the 60° sample has the smallest deformation. The 90° sample shows a downward bending toward the electromagnet, and other samples' downward bending angles are summarized in Figure 10d. The above results prove that the SM bianisotropic MSE sample can achieve off-plane deformation with different directions and angles by regulating the particle chain orientation and the external magnetic field.

Then, the SM bianisotropic MSE sample with off-plane 3D deformability is integrated with an infrared sensor module, developing a smart system with defense and sentry functions. The schematic is shown in Figure S16a, and its actuation module is composed of an electromagnet and an SM bianisotropic MSE sample. Once the infrared sensor recognizes the object, low-level output will trigger the relay. Then, the relay energizes the electromagnet and the sample deforms. As shown in Figures 10e and S16b, when the object enters the sensor's surveillance area, the sample deforms for signaling or defending (Video S5).

We next assemble these SM bianisotropic MSE samples into a network. A four-open switch based on the network bianisotropic MSE is demonstrated, taking the bianisotropic MSE's advantages of multimode deformation, being sensitive to the in-plane magnetic field, and the 3D deformation activated by an off-plane magnetic field. As shown in Figure S17, when the sample is in the initial state without any deformation, the four terminal pairs are all unconnected and LEDs are off. Applying a permanent magnet right above the copper foil on the sample (Figure S18a), an off-plane deformation of the sample causes the group 1 terminal pair to be connected and the green LED to light up. When the magnet reaches the front above the copper foil along the route shown in Figure S18b, the group 2 terminal pair is connected and the red LED lights up as a result of which the sample displays in-plane elongation and out-of-plane deformation. Figure S18c,d exhibits that when the magnet comes from ±45° diagonally above, the terminal pair on the yellow or blue LED circuit can be connected, which can be attributed to the flexibility and excellent 3D deformability of the sample. Repeated tests prove that the flexible magnetic switch is ingenious and durable (Video S6). Additionally, the orientation of the inclined particle chain could be designed to provide more multifold out-of-plane deformability for more appealing functions such as drug capture and reconfigurable flexible substrates using the network bianisotropic MSE.

3. CONCLUSIONS

In summary, we developed a novel soft magnetic particle-embedded shape material bianisotropic MSE composite with more excellent multimodal deformation response to the magnetic field magnitude and direction utilizing simple template sacrifice and a modular design. The shape anisotropy and the anisotropy of the internal microstructure contribute cooperatively to the magnetic anisotropy of the SM bianisotropic MSE. A beam magneto-deformation model considering demagnetization factors of SM bianisotropic MSE is proposed and reveals that the magnetic anisotropy makes the magneto-induced deformation sensitive to the magnetic field direction as MRE with hard magnetic particles. We systematically tested and, using the finite element method, verified the multimode transformations of various SM bianisotropic MSE assemblies that elongated or contracted under horizontal or vertical magnetic fields. The deformation amplitude can be controlled by magnetic field strength, and the response time is about 0.3 s. Compared with shape anisotropic MSE, the SM bianisotropic MSE shows multiplied deformability. The 3D transformations of SM bianisotropic MSE are also implemented by regulating the internal particle chain orientation during preparation. Finally, taking advantage of the SM bianisotropic MSE of being programmable, controllable, fast and excellent multideformation, we demonstrate the multifunctional applications in the logic switch for flexible electronics, magnetic manipulator for soft robotics, and actuation module for intelligent systems. The concept of the SM bianisotropic MSE could be extended to various magneto-sensitive elastomer systems, using shape memory polymers, thermally activated SMPs, dynamic polymer networks, and diverse magnetic particles, with shape locking, bifunctional, reconfigurable, and recyclable properties. With recent advances in simulating the optimization and 3D/4D printing and deposition technique, the application of different scale SM bianisotropic MSEs in bioengineering, morphological computing, active metamaterials, and next-generation soft robots can be expected.

4. EXPERIMENTAL SECTION

4.1. Materials. The mold used to prepare MSE is processed by 3D printing technology (Creator Pro 2, Flash Casting Technology Flagship Store). The printing accuracy is ±0.2 mm. The material used for printing is thermoplastic ABS. The melting point of ABS is 210−250 °C. CI particles (CN-type) with the diameter of about 7 μm were bought from BASF Aktiengesellschaft, Germany. The PDMS precursor and curing agent (Sylgard 184) were purchased from Dow Corning. All of the reagents were analytically pure and were adopted without additional purification.

4.2. Preparation of Shape Anisotropic MSE. The mold is first designed in SolidWorks 2016, converted into the STL format, and then printed out with the printer. When preparing the PDMS-based MSE, the PDMS precursor, the 1:20 cross-linking agent, and CI particles are added to a beaker according to mass ratio and manually stirred with a glass rod for 0.5 h to fully mix the mixture. Next, the mixture is placed in a vacuum chamber for 20 min followed by filling in the mold. After scraping off the excess part with a spatula, the mold filled with the mixture is vacuum-treated again for 10 min. Then, the mold is transferred to an oven, and the mixture is vulcanized at 80 °C for 2 h. Finally, the mold is dissolved with acetone ultrasonically, and the shape anisotropic MSE is obtained.

https://doi.org/10.1021/acsami.2c03533
ACS Appl. Mater. Interfaces 2022, 14, 20101−20112

4.3. Preparation of SM Bianisotropic MSE. The mold for preparing the MSE with a strip shape is printed; then, the mixture is filled in the mold followed by pumping vacuum. Next, the mold is placed in a 40 mT prestructured magnetic field for 10 min. The process that the CI particles are arranged in chains and the orientation of CI particles changes with the direction of the external magnetic field are observed using an optical microscope (Video S7). As a result, the CI particles in the mixture are arranged in chains along the long axis. The prestructured magnetic field generator is composed of a trestle and two electromagnets (XDA-120/70, Yueqing Xingda Electric Co., Ltd., China) powered by a DC power supply (ITECH IT6724). Then, the mold is transferred to the oven. After prevulcanization for 0.5 h, the SM bianisotropic MSE parts are demolded. Afterward, these parts are elaborately embedded into a new mold, and adjacent parts are connected with the mixture. It is heated and cured for 1.5 h. After acetone ultrasonically dissolves the new mold, the assembled SM bianisotropic MSE is obtained. An SM bianisotropic MSE part in which the particle chain is oriented along the long axis is defined as the 90° sample. Other MSE parts with the particle chain orientation deviated from the long axis direction by 10, 20, and 30° are also prepared and named the 80° sample, the 70° sample, and the 60° sample.

4.4. Characterization. The microstructures are observed by a scanning electron microscope (SEM, Gemini 500, Carl Zeiss Jena, Germany) under 10 kV. The magnetorheological properties are measured by a rheometer (Physica MCR 302, Anton Paar Co., Austria) with a magneto-controllable accessory. The samples (dimension: about Φ 20 mm × 1 mm) are sheared at a frequency of 1 Hz with an amplitude of 0.01%. The mechanical properties are explored using an electroforce dynamic system (TA ElectroForce 3200, TA Instruments). The samples (dimension: about 30 mm × 11.5 mm × 2 mm) are stretched at a strain rate of 0.01/s. The hysteresis loops are tested by MicroSense VSM. The dimension of the disk specimen is Φ 5 mm × 1 mm. The results that the particle chain orientation of the material anisotropic sample is parallel to, 45° from, and perpendicular to the direction of the tested magnetic field are defined as "anisotropy p", "anisotropy 45°", and "anisotropy v", respectively. The "isotropy p" and "isotropy v" represent the results of the material isotropic sample. Moreover, the shape anisotropic MSE (dimension: 6.66 mm × 0.65 mm × 0.5 mm) is also tested to consider the shape effect. When the shape anisotropic MSE's longitudinal direction is along the test magnetic field direction, a parallel magnetization curve "shape anisotropy p" is obtained. The result measured when the sample is rotated 90° is defined as a vertical magnetization curve "shape anisotropy v". All of the measurements are conducted in the air at room temperature (25 °C).

4.5. In-Plane Multimode Deformation of Anisotropic MSE. The deformations of shape anisotropic MSE and SM bianisotropic MSE are accomplished using a uniform magnetic field generated by the two electromagnets, of which the coil excitation current is regulated by the DC power supply. The magnetic flux density ranges from 0 to 450 mT. The minimum interval time between adjacent steps of the current is 50 ms. The whole deformation process of the sample is recorded using a high-resolution CCD camera (MV-CA016-10UM, Hikvision, China). The frame rates are set at 200.

The displacement field and strain field calculation under different magnetic fields are carried out by employing an open source 2D digital image correlation MATLAB program (Ncorr). Moreover, the image processing of the deformation response time experiment is executed in GOM Correlate Pro.

4.6. Fabrication of the SM Bianisotropic MSE-Based Flexible LED Circuit Switch. The flexible switch is fabricated by fixing Al wires on the MSE sample. First, thin copper sheets are glued on the sample; then, silver paste is applied to weld Al wires on the copper sheets. The other end of wires is connected with the circuit's positive and negative poles.

4.7. 3D Multimode Deformation of SM Bianisotropic MSE. The sample (15 mm × 5 mm × 1.5 mm) is placed on top of an electromagnet. The electromagnet provides an off-plane gradient magnetic field. The 3D multimode deformation of the sample is recorded with a camera.

4.8. Preparation of the Magnetically Controlled Flexible Quadruple Single Control Switch. The free end of the sample is coated with copper foil. An electrically insulating plastic plate is fixed at a position 4.5 mm away from the sample's upper surface. There are four terminal pairs on the plate (directly above, front above, and ±45° diagonally above). The terminal is made of copper foil and a wire connected to the LED.

4.9. Finite Element Analysis of Shape Anisotropic MSE. The in-plane multimode deformation of shape anisotropic MSE is simulated by software COMSOL Multiphysics. Their geometric models are reconstructed by SolidWorks 2016. The finite element analysis is established by coupling the magnetic field-no current module with the solid mechanic module. The magnetic force on the sample is first calculated by integration of the surface stress tensor on its boundaries. The deformation subjected to magnetic force is calculated by the solid mechanic module. The relative permeabilities of the sample and air are set as 1.3 and 1, respectively. The sample is set as linear elastic, where the elastic modulus and Poisson's ratio are 0.4 MPa and 0.49, respectively. The density is measured and set as 3 g/cm^3. These models adopt tetrahedral grids, and the element sizes of the girds are set as extremely fine.

■ ASSOCIATED CONTENT

Supporting Information

The Supporting Information is available free of charge at https://pubs.acs.org/doi/10.1021/acsami.2c03533.

Magnetization constitutive of the anisotropic MSE sample (Section S1); SEMs of magneto-sensitive elastomers (MSEs) with 50 wt % CI particles (Figure S1); cross-section comparison of the material isotropic sample, the anisotropic 90° sample, and the anisotropic 60° sample (Figure S2); SEM images of the material isotropic sample and the anisotropic 90° sample, and the related element mappings of Fe and Si (Figure S3); magnetization curves of pure CI and disk material isotropic and anisotropic MSEs (Figure S4); various shapes of anisotropic MSEs with different architectures (Figure S5); magneto-deformation of regular hexagon-shaped anisotropic MSE (Figure S6); strain results of deformed rhombic-shaped anisotropic MSE (Figure S7); *y*-direction deformation response of the rhombic-shaped anisotropic MSE to a vertical step magnetic field with different amplitudes (Figure S8); strain results of deformed regular hexagon-shaped anisotropic MSE (Figure S9); displacement and strain of a re-entrant honeycomb-shaped anisotropic MSE subjected to a magnetic field (Figure S10); deformation of regular hexagon-shaped material bianisotropic MSE (Figure S11); strain results of SM bianisotropic MSEs (Figure S12); illustrations of SM bianisotropic MSE-based switches corresponding to codes (1, 1), (1, 0), and (0, 1) of the alphabet switch array (Figure S13); comparison of solid MSE and SM bianisotropic MSE trapping a magnet (Figure S14); preparation of the material anisotropic $-\theta$ sample and the θ sample (Figure S15); schematic of a multifunctional module system (Figure S16); top view and front view of the SM bianisotropic MSE-based magnetic four-open switch (Figure S17); and effect of the magnetic four-open switch on different LEDs (Figure S18) (PDF)

Deformations of rhombic-shaped anisotropic MSE under different magnetic flux densities (Video S1) (MP4)

https://doi.org/10.1021/acsami.2c03533
ACS Appl. Mater. Interfaces 2022, 14, 20101−20112

Electronic switches based on SM bianisotropic MSE samples (Video S2) (MP4)

Reticulated SM bianisotropic MSE wrapping a magnet (Video S3) (MP4)

Magnetically assisted flexible gripper based on the SM bianisotropic MSE (Video S4) (MP4)

Multifunctional module system (Video S5) (MP4)

Four-open switch based on the network bianisotropic MSE (Video S6) (MP4)

Orientation of CI particles changing with the direction of the external magnetic field (Video S7) (MP4)

AUTHOR INFORMATION

Corresponding Authors

Yu Wang − *CAS Key Laboratory of Mechanical Behavior and Design of Materials, Department of Modern Mechanics, University of Science and Technology of China (USTC), Hefei 230027, P. R. China*; Email: wyu@ustc.edu.cn

Xinglong Gong − *CAS Key Laboratory of Mechanical Behavior and Design of Materials, Department of Modern Mechanics, University of Science and Technology of China (USTC), Hefei 230027, P. R. China*; orcid.org/0000-0001-6997-9526; Email: gongxl@ustc.edu.cn

Authors

Jingyi Zhang − *CAS Key Laboratory of Mechanical Behavior and Design of Materials, Department of Modern Mechanics, University of Science and Technology of China (USTC), Hefei 230027, P. R. China*

Huaxia Deng − *CAS Key Laboratory of Mechanical Behavior and Design of Materials, Department of Modern Mechanics, University of Science and Technology of China (USTC), Hefei 230027, P. R. China*

Chunyu Zhao − *CAS Key Laboratory of Mechanical Behavior and Design of Materials, Department of Modern Mechanics, University of Science and Technology of China (USTC), Hefei 230027, P. R. China*

Yanan Zhang − *IAT-Chungu Joint Laboratory for Additive Manufacturing, Institute of Advanced Technology, University of Science and Technology of China (USTC), Hefei 230027, P. R. China*

Haiyi Liang − *IAT-Chungu Joint Laboratory for Additive Manufacturing, Institute of Advanced Technology, University of Science and Technology of China (USTC), Hefei 230027, P. R. China*; orcid.org/0000-0001-7458-8036

Complete contact information is available at: https://pubs.acs.org/10.1021/acsami.2c03533

Notes

The authors declare no competing financial interest.

ACKNOWLEDGMENTS

X.G., J.Z., Y.W., H.D., and C.Z. received funding from the National Natural Science Foundation of China (Grant Nos. 11972337, 11972343, and 12132016) and Anhui's Key R&D Program of China (202104a05020009). Thanks to the instrumentation support from the engineering practice center of USTC.

ABBREVIATIONS

MSEs, magneto-sensitive elastomers

SM bianisotropic MSE, shape material bianisotropic magneto-sensitive elastomer

PDMS, poly(dimethylsiloxane)

CI, carbonyl iron

RVE, representative volume element

REFERENCES

(1) Wei, S.; Li, Z.; Lu, W.; Liu, H.; Zhang, J.; Chen, T.; Tang, B. Z. Multicolor Fluorescent Polymeric Hydrogels: Colorfulness Is More Shining Than Homochromy. *Angew. Chem., Int. Ed.* **2021**, *60*, 8608−8624.

(2) Cheng, X.; Zhang, Y. Micro/Nanoscale 3d Assembly by Rolling, Folding, Curving, and Buckling Approaches. *Adv. Mater.* **2019**, *31*, No. 1901895.

(3) Le, X.; Lu, W.; Zhang, J.; Chen, T. Recent Progress in Biomimetic Anisotropic Hydrogel Actuators. *Adv. Sci.* **2019**, *6*, No. 1801584.

(4) Lou, Z.; Li, L.; Wang, L.; Shen, G. Recent Progress of Self-Powered Sensing Systems for Wearable Electronics. *Small* **2017**, *13*, No. 1701791.

(5) Stano, G.; Percoco, G. Additive Manufacturing Aimed to Soft Robots Fabrication: A Review. *Extreme Mech. Lett.* **2021**, *42*, No. 101079.

(6) Burgert, I.; Fratzl, P. Plants Control the Properties and Actuation of Their Organs through the Orientation of Cellulose Fibrils in Their Cell Walls. *Integr. Comp. Biol.* **2009**, *49*, 69−79.

(7) Ding, L.; Pei, L.; Xuan, S.; Fan, X.; Cao, X.; Wang, Y.; Gong, X. Ultrasensitive Multifunctional Magnetoresistive Strain Sensor Based on Hair-Like Magnetization-Induced Pillar Forests. *Adv. Electron.* **2019**, *6*, No. 1900653.

(8) Qi, S.; Guo, H.; Fu, J.; Xie, Y.; Zhu, M.; Yu, M. 3d Printed Shape-Programmable Magneto-Active Soft Matter for Biomimetic Applications. *Compos. Sci. Technol.* **2020**, *188*, No. 107973.

(9) Erb, R. M.; Sander, J. S.; Grisch, R.; Studart, A. R. Self-Shaping Composites with Programmable Bioinspired Microstructures. *Nat. Commun.* **2013**, *4*, No. 1712.

(10) Wang, M.; Li, Q.; Shi, J.; Cao, X.; Min, L.; Li, X.; Zhu, L.; Lv, Y.; Qin, Z.; Chen, X.; Pan, K. Bio-Inspired High Sensitivity of Moisture-Mechanical Go Films with Period-Gradient Structures. *ACS Appl. Mater. Interfaces* **2020**, *12*, 33104−33112.

(11) Jeon, J.; Park, J. E.; Park, S. J.; Won, S.; Zhao, H.; Kim, S.; Shim, B. S.; Urbas, A.; Hart, A. J.; Ku, Z.; Wie, J. J. Shape-Programmed Fabrication and Actuation of Magnetically Active Micropost Arrays. *ACS Appl. Mater. Interfaces* **2020**, *12*, 17113−17120.

(12) El Helou, C.; Buskohl, P. R.; Tabor, C. E.; Harne, R. L. Digital Logic Gates in Soft, Conductive Mechanical Metamaterials. *Nat. Commun.* **2021**, *12*, No. 1633.

(13) Cai, L.; Chen, G.; Wang, Y.; Zhao, C.; Shang, L.; Zhao, Y. Boston Ivy-Inspired Disc-Like Adhesive Microparticles for Drug Delivery. *Research* **2021**, *2021*, No. 9895674.

(14) Han, J.; Jiang, W.; Niu, D.; Li, Y.; Zhang, Y.; Lei, B.; Liu, H.; Shi, Y.; Chen, B.; Yin, L.; Liu, X.; Peng, D.; Lu, B. Untethered Soft Actuators by Liquid-Vapor Phase Transition: Remote and Programmable Actuation. *Adv. Intell. Syst.* **2019**, *1*, No. 1900109.

(15) Liu, H.; Tian, H.; Shao, J.; Wang, Z.; Li, X.; Wang, C.; Chen, X. An Electrically Actuated Soft Artificial Muscle Based on a High-Performance Flexible Electrothermal Film and Liquid-Crystal Elastomer. *ACS Appl. Mater. Interfaces* **2020**, *12*, 56338−56349.

(16) Jolly, M. R.; Carlson, J. D.; Muñoz, B. C.; Bullions, T. A. The Magnetoviscoelastic Response of Elastomer Composites Consisting of Ferrous Particles Embedded in a Polymer Matrix. *J. Intell. Mater. Syst. Struct.* **1996**, *7*, 613−622.

(17) Yun, G.; Tang, S.-Y.; Sun, S.; Yuan, D.; Zhao, Q.; Deng, L.; Yan, S.; Du, H.; Dickey, M. D.; Li, W. Liquid Metal-Filled Magnetorheological Elastomer with Positive Piezoconductivity. *Nat. Commun.* **2019**, *10*, No. 1300.

(18) Kim, Y.; Yuk, H.; Zhao, R.; Chester, S. A.; Zhao, X. Printing Ferromagnetic Domains for Untethered Fast-Transforming Soft Materials. *Nature* **2018**, *558*, 274−279.
(19) Zhao, Z.; Wu, J.; Mu, X.; Chen, H.; Qi, H. J.; Fang, D. Origami by Frontal Photopolymerization. *Sci. Adv.* **2017**, *3*, No. 1602326.
(20) Wang, S.; Gao, Y.; Wei, A.; Xiao, P.; Liang, Y.; Lu, W.; Chen, C.; Zhang, C.; Yang, G.; Yao, H.; Chen, T. Asymmetric Elastoplasticity of Stacked Graphene Assembly Actualizes Programmable Untethered Soft Robotics. *Nat. Commun.* **2020**, *11*, No. 4359.
(21) Dagdeviren, C.; Joe, P.; Tuzman, O. L.; Park, K.-I.; Lee, K. J.; Shi, Y.; Huang, Y.; Rogers, J. A. Recent Progress in Flexible and Stretchable Piezoelectric Devices for Mechanical Energy Harvesting, Sensing and Actuation. *Extreme Mech. Lett.* **2016**, *9*, 269−281.
(22) Shintake, J.; Rosset, S.; Schubert, B.; Floreano, D.; Shea, H. Versatile Soft Grippers with Intrinsic Electroadhesion Based on Multifunctional Polymer Actuators. *Adv. Mater.* **2016**, *28*, 231−238.
(23) Martinez, R. V.; Fish, C. R.; Chen, X.; Whitesides, G. M. Elastomeric Origami: Programmable Paper-Elastomer Composites as Pneumatic Actuators. *Adv. Funct. Mater.* **2012**, *22*, 1376−1384.
(24) Yang, D.; Mosadegh, B.; Ainla, A.; Lee, B.; Khashai, F.; Suo, Z.; Bertoldi, K.; Whitesides, G. M. Buckling of Elastomeric Beams Enables Actuation of Soft Machines. *Adv. Mater.* **2015**, *27*, 6323−6327.
(25) Kim, Y. I.; An, S.; Yarin, A. L.; Yoon, S. S. Performance Enhancement of Soft Nanotextured Thermopneumatic Actuator by Incorporating Silver Nanowires into Elastomer Body. *Soft Rob.* **2021**, *8*, 711−719.
(26) Eshaghi, M.; Ghasemi, M.; Khorshidi, K. Design, Manufacturing and Applications of Small-Scale Magnetic Soft Robots. *Extreme Mech. Lett.* **2021**, *44*, No. 101268.
(27) Lee, K. H.; Yu, K.; Al Ba'ba'a, H.; Xin, A.; Feng, Z.; Wang, Q. Sharkskin-Inspired Magnetoactive Reconfigurable Acoustic Metamaterials. *Research* **2020**, *2020*, No. 4825185.
(28) Ze, Q.; Kuang, X.; Wu, S.; Wong, J.; Montgomery, S. M.; Zhang, R.; Kovitz, J. M.; Yang, F.; Qi, H. J.; Zhao, R. Magnetic Shape Memory Polymers with Integrated Multifunctional Shape Manipulation. *Adv. Mater.* **2020**, *32*, No. 1906657.
(29) Yu, K.; Fang, N. X.; Huang, G.; Wang, Q. Magnetoactive Acoustic Metamaterials. *Adv. Mater.* **2018**, *30*, No. 1706348.
(30) Roh, S.; Okello, L. B.; Golbasi, N.; Hankwitz, J. P.; Liu, J. A. C.; Tracy, J. B.; Velev, O. D. 3d-Printed Silicone Soft Architectures with Programmed Magneto-Capillary Reconfiguration. *Adv. Mater. Technol.* **2019**, *4*, No. 1800528.
(31) Montgomery, S. M.; Wu, S.; Kuang, X.; Armstrong, C. D.; Zemelka, C.; Ze, Q.; Zhang, R.; Zhao, R.; Qi, H. J. Magneto-Mechanical Metamaterials with Widely Tunable Mechanical Properties and Acoustic Bandgaps. *Adv. Funct. Mater.* **2020**, *31*, No. 2005319.
(32) Deng, H.; Sattari, K.; Xie, Y.; Liao, P.; Yan, Z.; Lin, J. Laser Reprogramming Magnetic Anisotropy in Soft Composites for Reconfigurable 3d Shaping. *Nat. Commun.* **2020**, *11*, No. 6325.
(33) Jiralerspong, T.; Bae, G.; Lee, J. H.; Kim, S. K. Wireless Control of Two- and Three-Dimensional Actuations of Kirigami Patterns Composed of Magnetic-Particles-Polymer Composites. *ACS Nano* **2020**, *14*, 17589−17596.
(34) Wu, S.; Hu, W.; Ze, Q.; Sitti, M.; Zhao, R. Multifunctional Magnetic Soft Composites: A Review. *Multifunct. Mater.* **2020**, *3*, No. 042003.
(35) Song, H.; Lee, H.; Lee, J.; Choe, J. K.; Lee, S.; Yi, J. Y.; Park, S.; Yoo, J. W.; Kwon, M. S.; Kim, J. Reprogrammable Ferromagnetic Domains for Reconfigurable Soft Magnetic Actuators. *Nano Lett.* **2020**, *20*, 5185−5192.
(36) Hu, W.; Lum, G. Z.; Mastrangeli, M.; Sitti, M. Small-Scale Soft-Bodied Robot with Multimodal Locomotion. *Nature* **2018**, *554*, 81−85.
(37) Chen, Z.; Lin, Y.; Zheng, G.; Yang, Y.; Zhang, Y.; Zheng, S.; Li, J.; Li, J.; Ren, L.; Jiang, L. Programmable Transformation and Controllable Locomotion of Magnetoactive Soft Materials with 3d-Patterned Magnetization. *ACS Appl. Mater. Interfaces* **2020**, *12*, 58179−58190.
(38) Xu, T.; Zhang, J.; Salehizadeh, M.; Onaizah, O.; Diller, E. Millimeter-Scale Flexible Robots with Programmable Three-Dimensional Magnetization and Motions. *Sci. Rob.* **2019**, *4*, No. eaav4494.
(39) Zhang, J.; Diller, E. Untethered Miniature Soft Robots: Modeling and Design of a Millimeter-Scale Swimming Magnetic Sheet. *Soft Rob.* **2018**, *5*, 761−776.
(40) Schmauch, M. M.; Mishra, S. R.; Evans, B. A.; Velev, O. D.; Tracy, J. B. Chained Iron Microparticles for Directionally Controlled Actuation of Soft Robots. *ACS Appl. Mater. Interfaces* **2017**, *9*, 11895−11901.
(41) Tsumori, F.; Saijou, A.; Osada, T.; Miura, H. Development of Actuation System for Artificial Cilia with Magnetic Elastomer. *Jpn. J. Appl. Phys.* **2015**, *54*, No. 06FP12.
(42) Mishra, S. R.; Dickey, M. D.; Velev, O. D.; Tracy, J. B. Selective and Directional Actuation of Elastomer Films Using Chained Magnetic Nanoparticles. *Nanoscale* **2016**, *8*, 1309−1313.
(43) Zhang, Y.; Wang, Q.; Yi, S.; Lin, Z.; Wang, C.; Chen, Z.; Jiang, L. 4d Printing of Magnetoactive Soft Materials for on-Demand Magnetic Actuation Transformation. *ACS Appl. Mater. Interfaces* **2021**, *13*, 4174−4184.
(44) Li, X.; Peng, Z.; Yang, Y.; Chen, S. Tunable Adhesion of a Bio-Inspired Micropillar Arrayed Surface Actuated by a Magnetic Field. *J. Appl. Mech.* **2019**, *86*, No. 011007.
(45) Chai, Z.; Liu, M.; Chen, L.; Peng, Z.; Chen, S. Controllable Directional Deformation of Micro-Pillars Actuated by a Magnetic Field. *Soft Matter* **2019**, *15*, 8879−8885.
(46) Tu, H.; Gao, Z.; Bai, C.; Lan, S.; Wang, Y.; Zhang, Q. Single-Camera 3d-Dic System Based on a Fiber Bundle. *Opt. Lasers Eng.* **2021**, *147*, No. 106743.
(47) Su, Y.; Zhang, Q. Glare: A Free and Open-Source Software for Generation and Assessment of Digital Speckle Pattern. *Opt. Lasers Eng.* **2022**, *148*, No. 106766.
(48) Novelino, L. S.; Ze, Q.; Wu, S.; Paulino, G. H.; Zhao, R. Untethered Control of Functional Origami Microrobots with Distributed Actuation. *Proc. Natl. Acad. Sci. U.S.A.* **2020**, *117*, 24096−24101.
(49) Lin, C.; Liu, L.; Liu, Y.; Leng, J. 4d Printing of Bioinspired Absorbable Left Atrial Appendage Occluders: A Proof-of-Concept Study. *ACS Appl. Mater. Interfaces* **2021**, *13*, 12668−12678.

https://doi.org/10.1021/acsami.2c03533
ACS Appl. Mater. Interfaces 2022, 14, 20101−20112